

RESEARCH ARTICLE

10.1002/2015JD023402

Key Points:

- AR5 ModelE2 had too much upper tropospheric CO during a major emissions event
- Changes to the subgrid physics significantly reduced this discrepancy
- Comparing against TES/MLS CO was a useful independent model test

Correspondence to:

R. D. Field,
robert.field@columbia.edu

Citation:

Field, R. D., M. Luo, D. Kim, A. D. Del Genio, A. Voulgarakis, and J. Worden (2015), Sensitivity of simulated tropospheric CO to subgrid physics parameterization: A case study of Indonesian biomass burning emissions in 2006, *J. Geophys. Res. Atmos.*, 120, doi:10.1002/2015JD023402.

Received 18 MAR 2015

Accepted 16 OCT 2015

Accepted article online 21 OCT 2015

Sensitivity of simulated tropospheric CO to subgrid physics parameterization: A case study of Indonesian biomass burning emissions in 2006

Robert D. Field^{1,2}, Ming Luo³, Daehyun Kim⁴, Anthony D. Del Genio¹, Apostolos Voulgarakis⁵, and John Worden³

¹NASA Goddard Institute for Space Studies, New York, New York, USA, ²Department of Applied Physics and Applied Mathematics, Columbia University, New York, New York, USA, ³Jet Propulsion Laboratory/California Institute of Technology, Pasadena, California, USA, ⁴Department of Atmospheric Sciences, University of Washington, Seattle, Washington, USA, ⁵Department of Physics, Imperial College London, London, UK

Abstract Recent cumulus and turbulence parameterization changes to the NASA GISS ModelE2 have improved representation of the Madden-Julian Oscillation and low cloud distribution, but their effect on composition-related quantities is not known. In this study, we simulate the vertical transport of carbon monoxide (CO) from uncontrolled biomass burning in Indonesia in late 2006, during which uniquely high CO was detected in the upper troposphere. Two configurations of ModelE2, one without the changes (AR5) and one with the changes (AR5'), are used for an ensemble simulation of the transport of CO from the biomass burning. The simulation results are evaluated against new CO profiles retrieved jointly from the Aura Tropospheric Emission Spectrometer and the Microwave Limb Sounder. Modeled upper tropospheric CO using the AR5 physics was unrealistically high. The AR5' physics suppress deep convection that reaches near the tropopause, reducing vertical transport of CO to the upper troposphere and bringing the model into better agreement with satellite CO. In this regard, the most important changes were related to the strength of entrainment of environmental air into the convective column, the strength of re-evaporation above cloud base, and a negative plume buoyancy threshold based on density temperature. This study illustrates how individual, noncomposition model changes can lead to significantly different modeled composition, which in this case improved agreement with satellite retrievals. This study also illuminates the potential usefulness of CO satellite observations in constraining unobservable processes in general circulation models.

1. Introduction

Early, limited upper tropospheric carbon monoxide (CO) measurements suggested that deep convection is a key mechanism through which CO is vertically transported from near the planetary boundary layer (PBL). Seiler and Fishman [1981] showed that along the west coast of the Americas, CO generally decreased with altitude, except for a narrow band coincident with the Intertropical Convergence Zone (ITCZ), which they attributed to polluted surface air being lifted to the mid and upper troposphere by ubiquitous convection over the ITCZ. The same mechanism has been proposed to explain high upper tropospheric CO over, for example, the Gulf of Guinea [Reichle et al., 1986], Oklahoma [Dickerson et al., 1987], and South America [Roths and Harris, 1996; Pickering et al., 1996; Andreae et al., 2001].

Our understanding of this transport pathway has improved with sustained remote sensing retrievals of pollutants in the troposphere. Elevated upper tropospheric CO from Measurements of Pollution in the Troposphere (MOPITT) over the Indian Ocean in 2003 could be attributed to the horizontal transport and progressive convective uplift of emissions from Australia, Indonesia, and Africa [Edwards et al., 2006]. Jiang et al. [2007] showed using observations made with Aura Microwave Limb Sounder (MLS) that upper tropospheric CO and its long-range transport over the Pacific peaked in the summer when convection was at its maximum. This was due to urban and industrial sources, rather than biomass burning emissions, which were suppressed during that period by heavy rainfall.

Huang et al. [2012] analyzed MLS and Aura Tropospheric Emission Spectrometer (TES) CO measurements for the entire 40°S to 40°N domain during 2007 and identified direct convective uplift of boundary layer air near emissions sources as the dominant source of elevated CO in the upper troposphere, as opposed to uplift of polluted air first advected from source regions. Livesey et al. [2013] showed consistent seasonal upper

tropospheric CO peaks over polluted regions from 2004 to 2011. Like *Jiang et al.* [2007], they noted that upper tropospheric CO is less likely to be related to biomass burning emissions directly coincident at the surface because deep convective precipitation will be simultaneously suppressing fire activity.

Modeling the relationships among emissions, transport, and chemistry is a challenge but necessary to understand the impacts of emissions. Our interest is in parameterized turbulent and convective processes that drive subgrid-scale convection, which remains a major source of uncertainty in global-scale models of the atmosphere [e.g., *Arakawa*, 2004; *Sherwood et al.*, 2014] that limits the accuracy of simulated emissions fate. *Chatfield et al.* [1998], for example, required an arbitrary 150% increase in parameterized cloud base mass flux for CO at the surface to reach the upper troposphere, but this required an increase in emissions to maintain reasonable CO concentrations in the lower troposphere. The simulated seasonal CO cycle in *Abad et al.* [2011] was less evident than in ACE-FTS CO retrievals, which was attributed either to underestimated biomass burning emissions or too little fast vertical transport. *Park et al.* [2013] arrived at a similar conclusion using the WACCM model driven by MERRA meteorology over South America. *Liu et al.* [2010] found that the modeled upper tropospheric CO in 2005 over South America using Goddard Earth Observing System version 4 (GEOS-4) assimilated meteorology peaked in November rather than in October as observed by MLS, due to emissions from the surface being detrained at too low an altitude. This was exacerbated for simulations using GEOS-5 assimilated meteorology, which has a different convection scheme, due to the late arrival of convective activity.

Errors in vertical transport therefore place a hard limit on agreement between modeled and observed CO. Worse, emissions adjustments can be compensating for errors in vertical transport. Model-data agreement might be improving but possibly for the wrong reasons. These problems can be understood to some extent with a Chemical Transport Model (CTM) through diagnosis and by conducting simulations with different prescribed meteorology. But to fully understand the specific contributions of different underlying processes to vertical pollutant distribution, the components of the model's parameterization must be examined individually.

The purpose of this study is to do so using experiments with the NASA GISS ModelE2 composition-climate model (CCM) evaluated against satellite retrievals of CO in the troposphere. *Ott et al.* [2011] demonstrated this approach using the GEOS-5 general circulation model (from which the GEOS-5 assimilated meteorology originates) equipped with basic CO chemistry for a free-running atmosphere with no assimilation of observations. We focus on the parameterized moist convection and turbulence because they dominate subgrid-scale vertical transport in the CCM. Changes are drawn from those that recently led to simulating a Madden-Julian Oscillation (MJO) in ModelE2 [*Kim et al.*, 2012] and slightly improved marine stratocumulus [*Yao and Cheng*, 2012]. *Field et al.* [2014] evaluated different model versions including these changes against water vapor isotope retrievals from TES, finding that the *Kim et al.* [2012] and *Yao and Cheng* [2012] modifications led to considerably better agreement in the tropical lower free troposphere.

Our goals are to determine the following: (1) if the choice of subgrid physics affects the vertical distribution of CO in ModelE2 during a major CO emissions event in 2006 over Indonesia and (2) the pathways through which modeled CO arrives in the upper troposphere from the source region and their dependence on subgrid physics.

2. Experiments and Data

We examine the emissions episode that occurred in Indonesia from September to November 2006. Due to combined El Niño and positive Indian Ocean Dipole conditions, a stronger and longer dry season led to uninterrupted biomass burning in degraded peatlands [*Field and Shen*, 2008; *van der Werf et al.*, 2008; *Field et al.*, 2009]. Figure 1 shows the Global Fire Emissions Database (GFED) CO estimates from July to December 2006 over the primary burning region in south central Sumatra and Kalimantan (Indonesian Borneo).

The event is an important natural experiment for understanding the roles of emissions, transport, and chemistry in controlling the vertical distribution of pollutants. Mean October 2006 TES CO at 511 hPa exceeded 200 ppbv over the region [*Logan et al.*, 2008]. *Lai et al.* [2011] attributed upper tropospheric CO enhancements of up to 200 ppbv measured in situ over the Philippines to the burning. The 2004–2011 MLS record of *Livesey et al.* [2013] showed that normally, upper tropospheric CO over Indonesia has a weaker seasonal peak compared to biomass burning regions in South America, northern Africa, or southern Africa, because during most years the dry seasons in this part of Indonesia are still wet enough to suppress severe burning. The 2006 event, however, stands out over the tropics as among the strongest during the MLS period. In

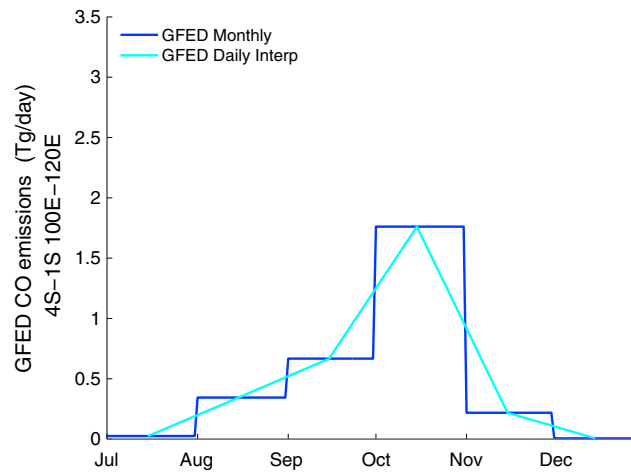


Figure 1. GFED CO emissions over the region identified in Figure 2b. Shown are the monthly mean estimates and the daily interpolation of those estimates used as input to ModelE2.

modeling the event, previous studies have shown strong sensitivity to whether deep convective transport is included [Nassar *et al.*, 2009] and to the choice of prescribed meteorology [Zhang *et al.*, 2011]. Worden *et al.* [2013] showed that after making an inversion-based estimate of CO emissions during the event using MOPITT profiles as a top-down constraint, residual errors had significant vertical structure, which was attributed to vertical transport errors in the GEOS-Chem CTM, in their case run with GEOS-5 meteorology.

The appeal of studying this event with a model is the combination of an unusually large emissions source near sharp gradients in convective activity and the availability of a new joint Aura TES/MLS

CO retrieval against which to make comparisons. The CO acts as a measurable, relatively insoluble tracer influenced strongly by complex processes in the model whose representation is continually being developed. The large signal resulting from an isolated CO tracer source at the surface should make any transport dependence on subgrid physics stand out from background noise.

We conducted simulations from June to December 2006 using the GISS ModelE2 composition-climate model [Shindell *et al.*, 2013; Schmidt *et al.*, 2014], with a 2° latitude by 2.5° longitude horizontal resolution and 40 vertical layers from the surface to 0.1 hPa. Tropospheric/stratospheric chemistry includes 156 chemical reactions among 51 gas species, while the aerosol scheme includes prognostic simulations of the mass distributions of sulfate, sea-salt, dust, and carbonaceous aerosols [Koch *et al.*, 2006, 2007]. Photolysis rates are simulated using the Fast-J2 scheme [Wild *et al.*, 2000], which accounts for the effects of modeled overhead ozone, clouds, aerosols, and surface reflections. The model's skill in capturing key tropospheric gaseous constituents and aerosols has been evaluated and shown to be realistic [Koch *et al.*, 2006; Voulgarakis *et al.*, 2011; Shindell *et al.*, 2013]. The model has also been shown to represent tropospheric OH reasonably well, when compared to other models and to observation-based estimates [Voulgarakis *et al.*, 2013]. Aerosols in the model are radiatively active, and the first indirect effect is included. Biomass burning emissions come from the monthly resolution version of the Global Fire Emissions Database 3 (GFED3) [van der Werf *et al.*, 2010] and were assumed to be uniformly mixed throughout the boundary layer upon release. Anthropogenic emissions of nonbiomass burning gases and aerosols come from Lamarque *et al.* [2010] and vary from decade to decade, with linear interpolation for intermediate years. Well-mixed greenhouse gas concentrations vary according to global mean observed values.

A number of modifications have been made to the convective parameterization, which are summarized in Table 1. We refer to the physics in Schmidt *et al.* [2014] as the AR5 version of the model and the physics with the Kim *et al.* [2012] and Yao and Cheng [2012] changes as the AR5' version of the model. The AR5' changes are (i) the removal of the entrainment limiter, which sets the fractional entrainment rate to zero whenever the mass of the updraft plume entering a layer exceeds the mass of the cloud base layer, (ii) the increase of the fractional entrainment rate coefficient of the less diluted plume from 0.3 to 0.4, (iii) allowing more rain re-evaporation by limiting the maximum amount of condensate used in the downdraft to half of the total condensate and by allowing the rain re-evaporation to occur in entire plume levels instead of only below cloud base, and (iv) using density temperature (virtual potential temperature including water vapor and cloud condensate) instead of potential temperature in calculating downdraft buoyancy.

In total, we ran nine experiments. We started with the AR5 version of the model as the control and then ran experiments where single parameterization changes from Table 1 were made (i.e., the changes did not "accumulate" toward AR5'). We also included an experiment where all changes to the cumulus parameterization were made together (but without changes to the turbulence scheme) and, finally, an experiment where all

Table 1. Changes to Convection and Turbulence in ModelE2^a

Parameter	Description	AR5	AR5'
T_p	Buoyancy threshold for downdraft initiation	Potential temperature	Density temperature (virtual potential temperature including water vapor and cloud condensate)
NewCldBaseEntrLmt	Limits on entrained mass at each layer	Entrained mass at each layer limited to that of plume base layer	Entrained mass at each layer limited to mass of that layer
Plume1Entr0.4	Entrainment coefficient for less diluted plume	0.3	0.4
RevpAboveCldBase	Extent of rain evaporation into environment	Below cloud only	Entire depth of plume
LessDDraftRevp	Downdraft re-evaporation limit	All condensate allowed to re-evaporate	50% of condensate allowed to re-evaporate
ATURB	Vertical turbulent flux	Diffusive and counter-gradient terms from <i>Holtlag and Moeng</i> [1991]	Diffusive and counter-gradient terms from <i>Holtlag and Boville</i> [1993]
	Turbulent length scale	<i>Holtlag and Boville</i> [1993]	<i>Holtlag and Boville</i> [1993] above PBL, <i>Nakanishi</i> [2001] within PBL including buoyancy length scale dependent on TKE
	PBL height diagnosis	Turbulent kinetic energy profile	Bulk Richardson number criterion from <i>Holtlag and Boville</i> [1993]

^aThe AR5 version of the model is described in *Schmidt et al.* [2014]. The entrainment and re-evaporation changes are discussed in detail in *Kim et al.* [2012] and the turbulence-related changes in *Yao and Cheng* [2012].

AR5' changes were made. All experiments were run with observed sea-surface temperatures prescribed as the boundary conditions. For each configuration, 12 ensemble members with randomly perturbed initial atmospheric temperature conditions were run to separate the physics response from meteorological noise, similar to *Ott et al.* [2011]. Most diagnosis was focused on the AR5 and AR5' end-member experiments.

We compared model CO to a new joint Aura TES/MLS retrieval [*Luo et al.*, 2013]. The Aura CO profile data are the retrieval product using combined TES and MLS spectral measurements taken at the nearest TES nadir and

October 2006 precipitation

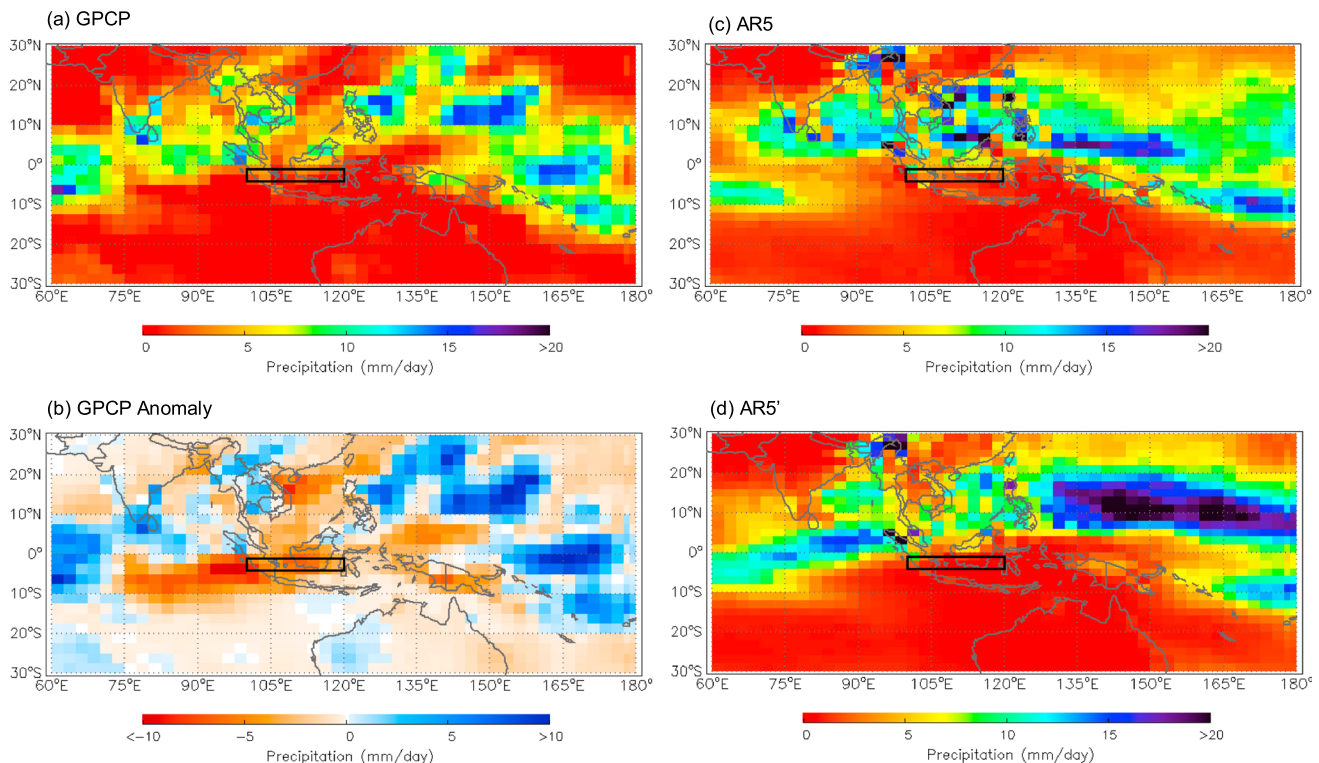


Figure 2. October 2006 precipitation for (a) GPCP v2.2, (b) GPCP departure anomaly from 1981 to 2010 long-term mean, (c) AR5, and (d) AR5'. The AR5 and AR5' precipitation are the means across 12 ensemble members. The black boxes indicate the emissions source region.

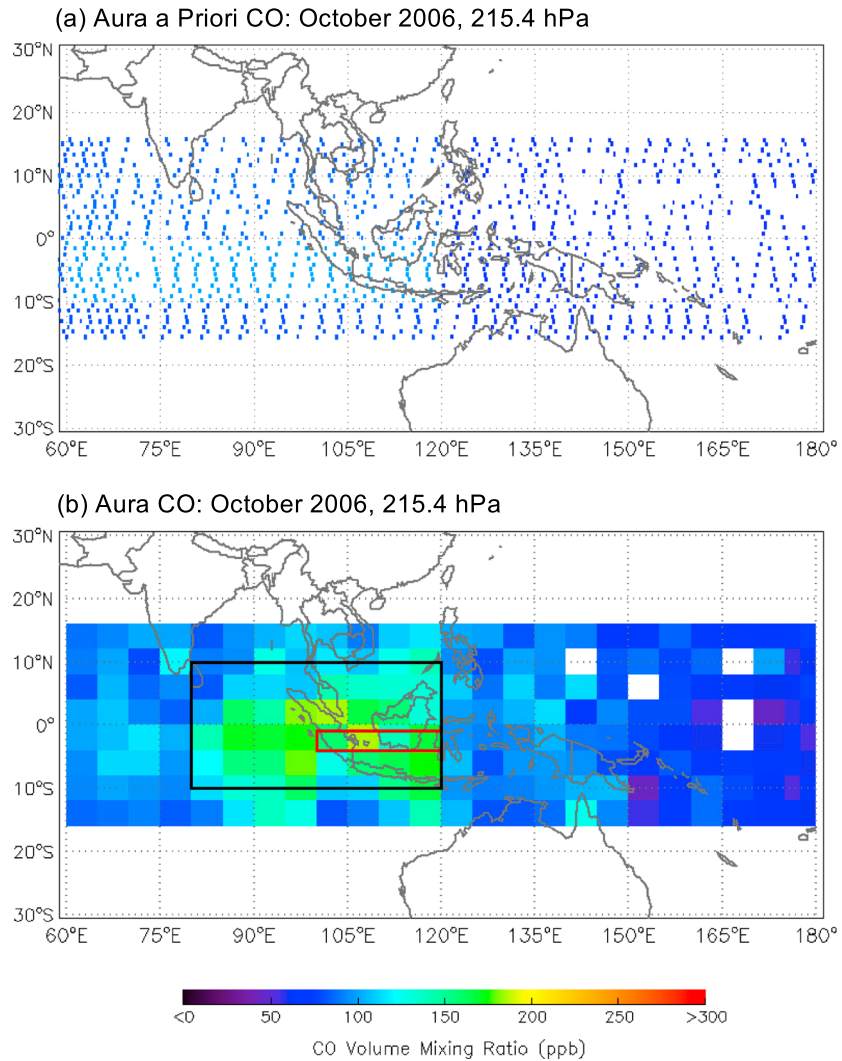


Figure 3. (a) October 2006 Aura CO prior at 215.4 hPa and (b) cell-averaged retrieval. The red box in Figure 3b indicates the emissions region.

MLS limb tangent locations. In the lower troposphere, TES measurements provide CO retrieval information. In the upper troposphere and lower stratosphere, the measurements from both instruments provide CO retrieval information. The joint retrievals in this range extend MLS data downward and increase sensitivity compared to the TES-alone retrievals. Comparisons of TES alone, MLS alone, and the combined Aura CO retrievals to colocated in situ balloon measurements illustrate the advantage of the Aura CO [Luo et al., 2013]. Preliminary validation of Aura CO against HIPPO and MOZAIC data sets indicates that the Aura CO is 20–30% lower over 300–200 hPa compared to the in situ data [Luo et al., 2014] which should be taken into account for model comparisons.

The estimate of the atmospheric constituent profiles from remote sensing measurements is described by the a priori profile and the averaging kernels. The proper way to compare retrieved and modeled CO is to estimate the instrument-equivalent profile via the retrieval process. Where noted, we first sample the model data at the Aura locations and times. The Aura CO retrieval operators are then applied to the model profiles:

$$x = X_a + A(X_{mod} - X_a)$$

where X_{mod} is the model profile, X_a is the a priori profile used in Aura CO retrieval, and A is the averaging kernel. x is obtained to compare to the Aura CO.

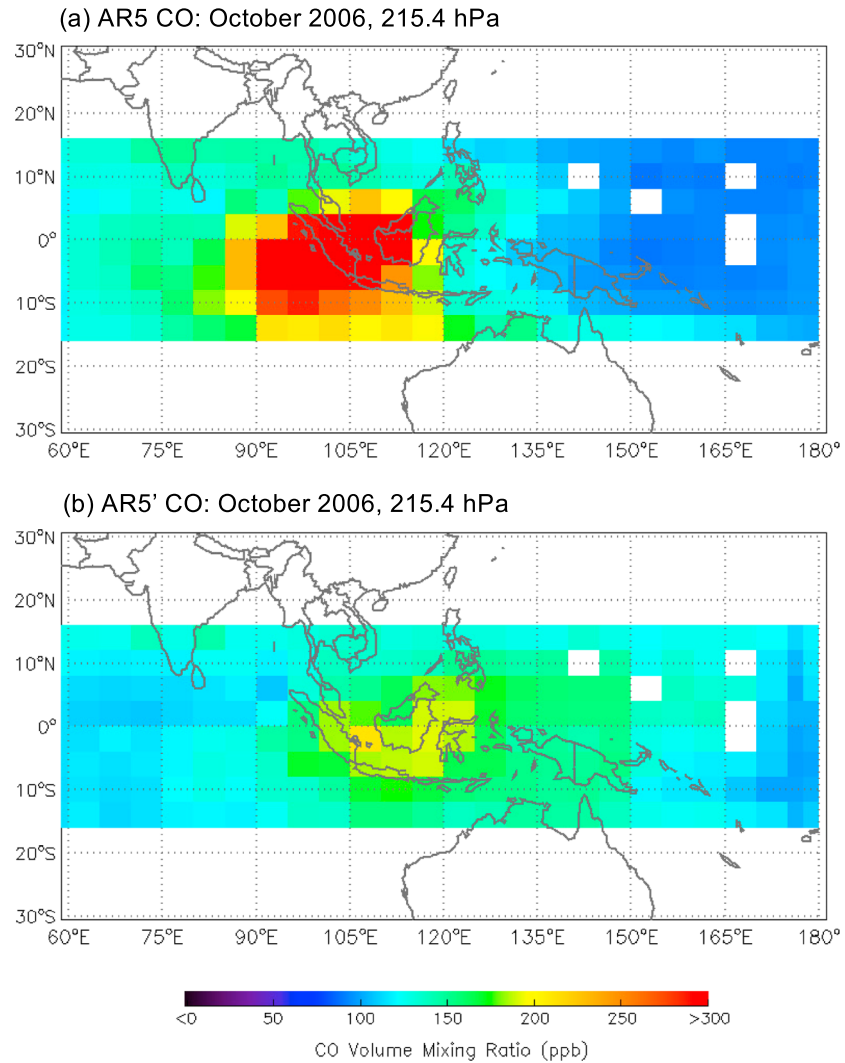


Figure 4. October 2006 ModelE2 AR5 CO at 215 hPa for (a) AR5 and (b) AR5', averaged across 12 perturbed initial condition ensemble members. The Aura operator has been applied to raw model CO output.

Table 2. October 2006 ModelE2 CO (ppbv) Statistics Over 10°S to 10°N, 80°E to 120°E Between 100 hPa and 287 hPa, the Black Box Shown in Figure 3b, for Raw Model Fields and Model Fields After Applying the Aura Operator^a

Experiment	Raw CO			CO With Aura Operator		
	Mean	Std	95% C.I. on Difference	Mean	Std	95% C.I. on Difference
AR5 (CTRL)	238.0	17.5	–	208.8	10.3	–
AR5_ATURB	219.5	10.6	(4.9, 32.1)	190.9	8.9	(10.3, 25.6)
AR5_EntrMassLim	210.3	13.7	(16.3, 39.1)	180.2	7.4	(19.1, 38.2)
AR5_T _p DDrft	196.2	19.1	(29.7, 53.9)	174.1	9.2	(26.1, 43.3)
AR5_RevAboveCldBase	193.8	11.2	(34.3, 54.0)	175.2	10.9	(25.6, 41.7)
AR5_HighEntCoef	225.9	14.6	(–2.9, 27.1)	216.4	14.3	(–17.4, 2.3)
AR5_LessDDrftRvp	232.1	20.5	(–10.6, 22.3)	204.2	13.9	(–6.9, 16.1)
AR5_CumulusChanges	162.0	13.4	(63.9, 88.1)	145.1	9.7	(56.2, 71.2)
AR5'	163.8	12.2	(62.6, 85.9)	143.3	8.9	(58.9, 72.0)
Aura				124.2		

^aThe standard deviation is that across the monthly means of the 12 ensemble members for each experiment. The 95% confidence interval (C.I.) is that of the difference between each experiment and AR5 (CTRL). Experiments with confidence intervals spanning zero are considered not statistically different from the AR5 experiment. The mean Aura CO for October 2006 is in the last row.

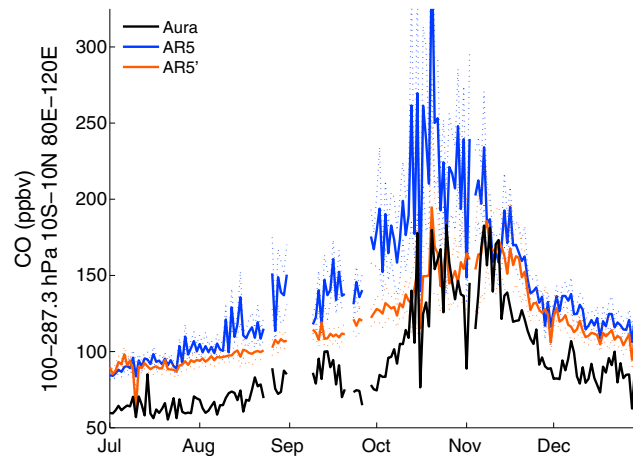


Figure 5. Regional upper tropospheric CO for Aura, AR5, and AR5'. The Aura operator has been applied to the model CO profiles. Solid line shows mean of 12 ensemble members, and dashed lines show 1-sigma variation across members.

was the result of the dry anomaly stretching across Indonesia in Figure 2b, which had in fact first appeared in July. AR5' (Figure 2d) has less (2.1 mm/d) precipitation than AR5 (3.5 mm/d) (Figure 2c) over the source region. AR5' is closer to the GPCP estimate of 1.7 mm/d, but the difference between AR5' and AR5 is small compared to regional gradients.

Figure 3 shows the Aura joint TES/MLS prior and retrieved CO at 215 hPa for October 2006 when the emissions peaked. The orbital sampling pattern in Figure 3a provides a sense of the density of the data used to construct the gridded Aura CO estimate in Figure 3b. The mean October 2006 CO over 10°S to 10°N, 80°E to 120°E between 100 hPa and 287 hPa was 124 ppbv, which was the most pronounced anomaly during the MLS period [Livesey *et al.*, 2013] in terms of magnitude, extent, and duration. Higher CO in western Indonesia than in the east is also the case for the duration of the episode through mid-November [Livesey *et al.*, 2013]. The red box in Figure 3b shows the primary emissions region. The black box in Figure 3b shows the region over which we focus comparison between Aura and ModelE2 CO in the upper troposphere. Quantitative comparison of ModelE2 CO was focused on the October 2006 ensemble average over this region rather than cell-by-cell variability within the region.

Figure 4 shows the October 2006 simulated CO for AR5 and AR5'. Model CO fields are sampled at Aura locations, and vertical profiles are smoothed with averaging kernels. The missing values in the western Pacific are due to gaps in the observed sampling coverage (Figure 4). In Table 2, we list the mean October 2006 CO over the upper tropospheric analysis region (the black box in Figure 3b) for AR5, AR5', and the intermediate experiments. Statistics are provided for the raw model CO profiles and the model profiles after applying the Aura operator. The standard deviation is that of the mean regional CO across the 12 ensemble members for each physics perturbation experiment (and not across individual, daily grid cells). The 95% confidence interval is that of the difference between AR5 and each perturbation. Experiments with confidence intervals that span 0 have mean upper tropospheric CO not significantly different from AR5 at the 95% confidence level.

ModelE2 CO at 215 hPa is generally higher than Aura for AR5, in particular over Indonesia where model values are well in excess of 300 ppbv. Over the analysis domain in Figure 3b, mean CO across the 12 AR5 ensemble members after applying the Aura operator is 209 ppbv. ModelE2 with AR5' physics still has a positive CO bias, but the peak values over Indonesia are brought into better agreement with Aura CO, as is the mean of 143 ppbv across ensemble members. The 66 ppbv difference between AR5 and AR5' across ensemble members is statistically significant at the 95% level (Table 2). There is also a weaker CO gradient between Indonesia and the Pacific for AR5', possibly due to changes in upper tropospheric circulation induced by the convective changes.

Figure 5 shows the evolution of the Aura, AR5, and AR5' upper tropospheric CO over the large domain from the start of localized burning in August, to the October peak, to the full return of the monsoon in December 2006. The Aura operator has been applied to model CO fields before taking the mean across the 12 ensemble

3. Results

3.1. Basic Event Characterization for Aura and ModelE2

For meteorological context, and to provide a sense of where the active convection is, Figure 2 shows the October 2006 GPCP precipitation, GPCP precipitation anomaly, and the AR5 and AR5' precipitation, both averaged across the 12 ensemble members. AR5 (Figure 2c) and AR5' (Figure 2d) both show an east-west arc of precipitation centered over the South China Sea corresponding qualitatively to the GPCP estimate (Figure 2a). The largest difference between AR5 and AR5' is over the western Pacific. The black boxes show how close the emissions were to the convective activity to the north over the South China Sea. The severe burning

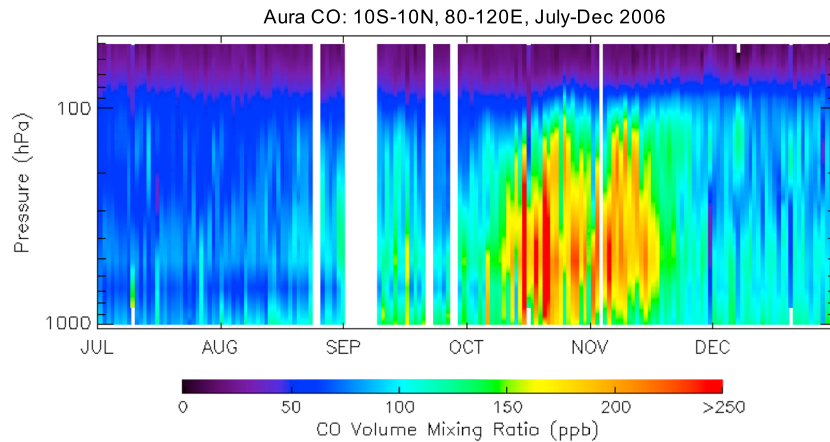


Figure 6. Regional time-height Aura CO.

members of each experiment. The large day-to-day variability of the AR5 and AR5' fields is due to the sparse sampling of the Aura operator shown in Figure 3a. Modeled upper tropospheric CO reflects the emissions changes in Figure 1 but modulated by the different transport between experiments. In July, before serious burning has started, AR5 and AR5' background CO is ~80 ppbv compared to ~55 ppbv for Aura. For AR5, this bias increases more rapidly as the event builds up. The difference between AR5 and AR5' CO grows as the emissions increase in August and September, peaking in October. Especially if we allow for a 20–30% low Aura CO bias in the upper troposphere, the AR5' CO is brought into better agreement with Aura. The raw model CO without the Aura operator (not shown) evolves similarly to that in Figure 5, but with higher upper

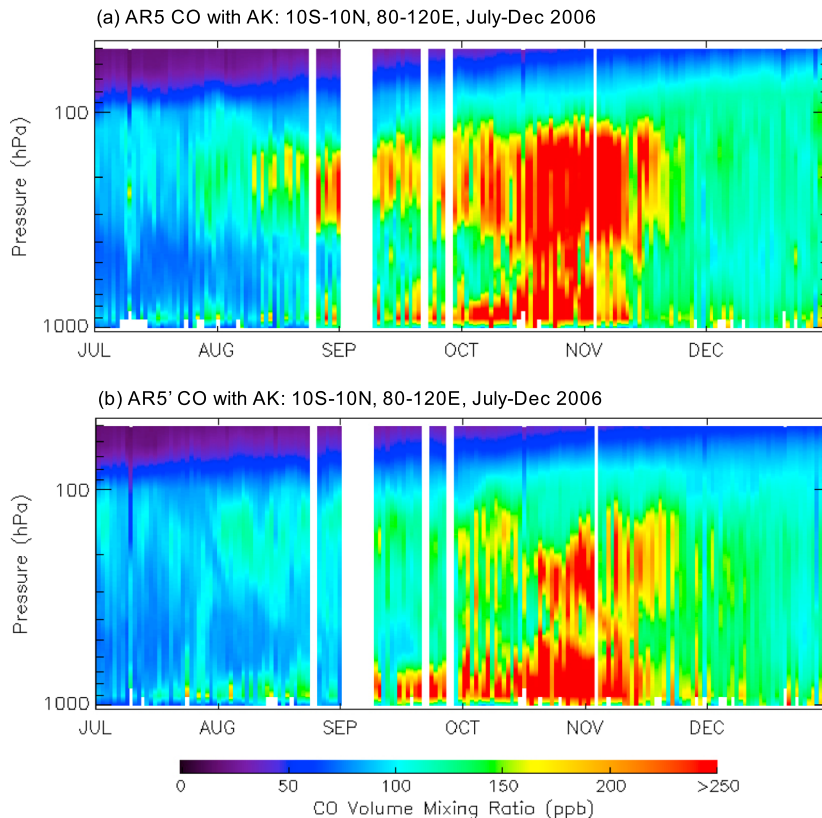


Figure 7. Regional time-height ModelE2 CO for (a) AR5 and (b) AR5'. Model fields have been sampled at Aura locations but without averaging kernel smoothing.

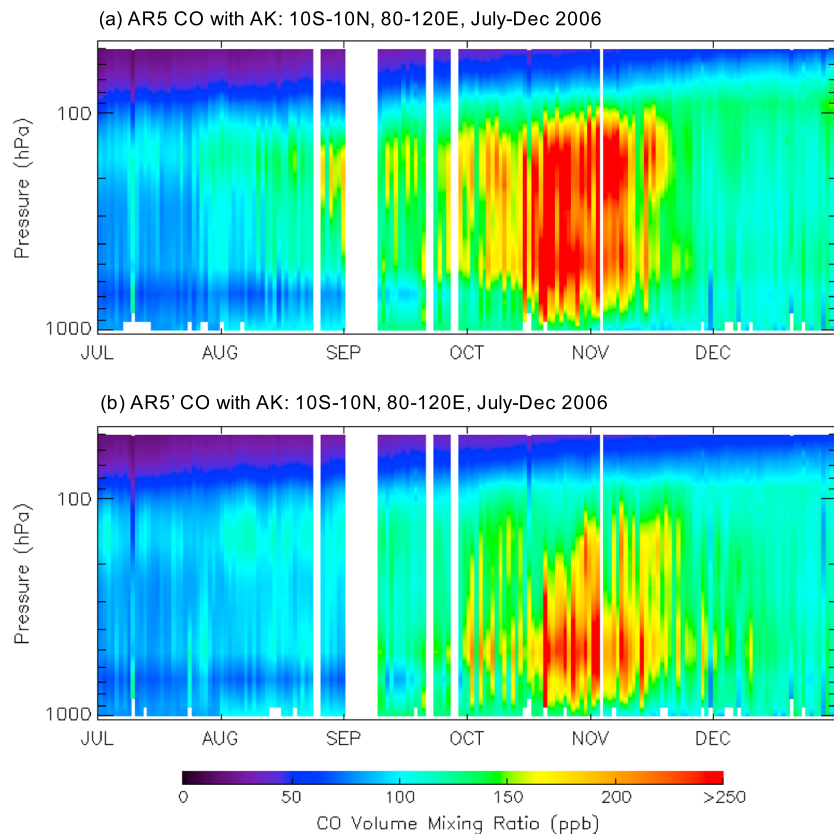


Figure 8. Same as Figure 7 but with Aura averaging kernel smoothing.

tropospheric CO (Table 2) that would not be resolved by Aura and less day-to-day variability due to the absence of location sampling.

Figure 6 shows the Aura time-height CO evolution over the same horizontal region as Figure 5. There is also high CO in the midtroposphere (Figure 6), consistent with *Logan et al.* [2008]. Figure 7 shows the ModelE2 time-height CO evolution with Aura location sampling but no averaging kernel smoothing of the raw model CO, to provide a sense of how the model distributes CO from the surface during the event. Differences in CO between AR5 and AR5' in the upper troposphere are greater than in the lower troposphere. By December, burning has stopped, the tracer source is removed, and AR5 and AR5' reconverge toward a background CO higher than in July, which presumably reflects ambient, residual CO from the event. Figure 8 is the same as Figure 7 but with averaging kernel smoothing as in Figures 4 and 5, which allows for comparison against the Aura vertical profile in Figure 6. Much of the vertical structure in the raw model output is smoothed away. For both AR5 and AR5', high CO close to the surface in the raw model output (Figure 7) is absent in the smoothed model CO because of the retrieval's decreasing sensitivity toward the surface. Despite this loss in vertical detail, differences between AR5 and AR5' CO are still apparent, and AR5' (Figure 8b) is in better agreement with Aura (Figure 6).

3.2. Differences in Convective CO Transport Between AR5 and AR5'

Previous studies have related upper tropospheric CO variability to proxies of deep convective transport such as cloud top height [*Zhang et al.*, 2011] and ice water content [*Livesey et al.*, 2013]. Similarly, lower precipitation over the source region in AR5' (Figure 2d) compared to AR5 (Figure 2c) hints at the role of convection in reducing upper tropospheric CO for AR5'. To isolate the role of convection, we diagnosed the CO tendency due to parameterized convection. The diagnosed quantity captures the net effects on CO of all parameterized convection processes: updrafts, downdrafts, entrainment from the environment into updrafts and downdrafts and vice versa, plume-top detrainment into the large-scale environment, and compensating within-grid cell subsidence. Positive tendencies indicate a net convective supply into a region across these processes, and negative tendencies indicate a net loss.

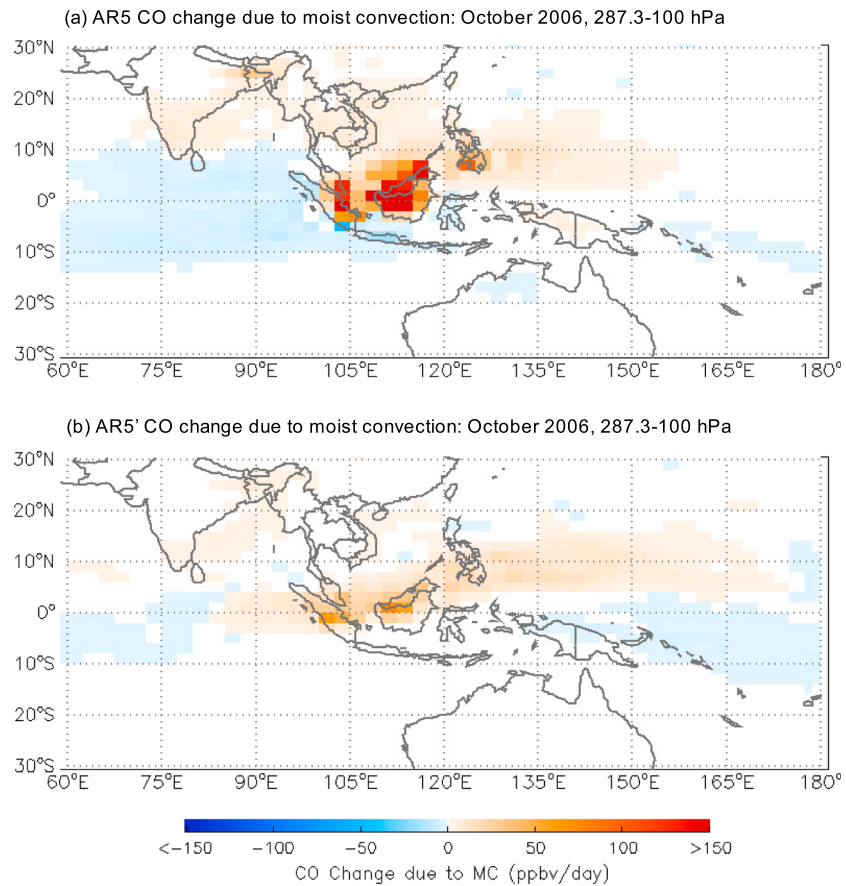


Figure 9. Mean October 2006 upper tropospheric CO tendency due to convective processes for (a) AR5 and (b) AR5'.

Figure 9 shows the mean upper tropospheric CO tendency due to convection for AR5 and AR5' for October 2006. This is the mean of the change in upper tropospheric CO due to all convective processes computed at each time step. More CO is supplied to the upper troposphere by convection for AR5 (Figure 9a). The region of positive CO convective tendency is centered slightly to the north of the source region for both experiments and is weaker for AR5'. At the surface, there is strong southerly flow over the source region for AR5 and AR5' (not shown), suggesting that some of the emissions are advected toward more convectively active regions to the north over the South China Sea, as indicated by the precipitation fields in Figures 2c and 2d.

Figure 10 shows time-height CO convective tendency over the source region spanning southern Sumatra and southern Kalimantan (rather than the larger domain in Figures 6–8). For AR5 (Figure 10a), as the burning increases in August, there is net convective CO loss near the surface and a gain in upper troposphere. When the CO emissions peak in October, the mean convective tendency for AR5 from the surface to 850 hPa is -189 ppbv/d and more CO is supplied to the upper troposphere than the lower free troposphere. For AR5' (Figure 10b), convective loss from the surface is much weaker than AR5 in August and September and only increases in mid-October with the southward migration of the ITCZ. During the October emissions peak, the mean convective CO tendency is -64 ppbv/d for AR5' and more CO is supplied to the lower free troposphere (~ 700 hPa) than to the upper troposphere. In the upper troposphere, the mean October convective tendency of CO is 71 ppbv/d for AR5 and 17 ppbv/d for AR5', and the difference between the two is statistically significant at the 95% level across the 12 ensemble members.

Figure 11 is the same as Figure 10 but north of source region, where there was also a strong supply of CO to the upper troposphere. There is steady net convective CO loss near the surface from July to September for both experiments. During the October emissions peak, net convective loss from the surface to 850 hPa for AR5' is stronger (-189 ppbv/d) than AR5' (-61 ppbv/d), which reflects weaker loss in AR5' at the beginning

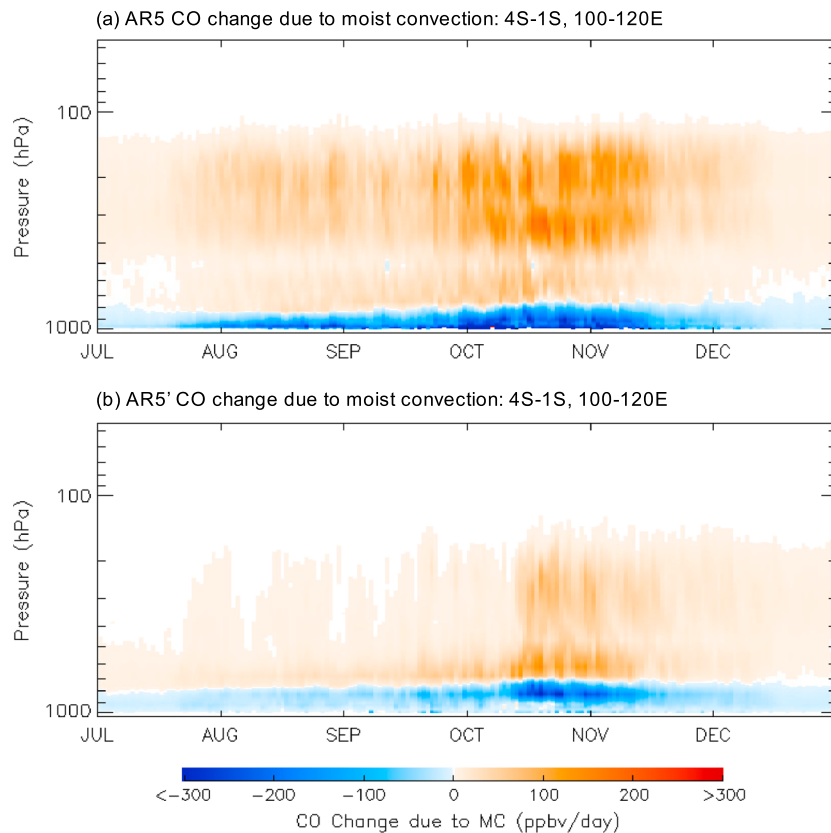


Figure 10. Time-height plot of CO tendency due to convection over source region for (a) AR5 and (b) AR5'.

of the month and a narrow band of CO supply to the surface at the end of the month. In the upper troposphere, the mean October convective tendency of CO is 91 ppbv/d for AR5 and 31 ppbv/d for AR5', and the difference between the two is statistically significant at the 95% level. During the October burning peak, AR5 convective supply to the upper troposphere is in fact 20 ppbv stronger than over the source region (Figure 10a). For AR5' (Figure 11b), most CO is supplied to the lower free troposphere rather than upper troposphere, similar to the source region. Up until mid-October, the height of maximum CO convective tendency in AR5' is between 500 hPa and 800 hPa, compared to between 200 hPa and 400 hPa for AR5. After mid-October for AR5', there is a greater mix between CO supplied to the lower troposphere and upper troposphere. The small net downward supply to the surface illustrates that CO transported downward through either downdrafts or within-grid cell compensating subsidence is non-negligible and that we are diagnosing the net vertical transport of sometimes competing processes.

Figure 12 shows that over intermediate experiments spanning AR5 to AR5', there is a strong positive relationship between convective CO tendency from north of the source region and regional CO in the upper troposphere. Much of the CO variability across the large domain without any other large sources can be explained by the convective transport over a relatively small region close to the emissions source. Upper tropospheric CO changes over the analysis domain in Figure 3b are listed in Table 2. The biggest single changes from the raw AR5 average of 238 ppb are due to the new entrainment mass limiter (AR5_EntrMassLim, 210 ppb), more re-evaporation above cloud base (AR5_RevAboveCldBase, 194 ppb), and a negative buoyancy threshold for downdraft initiation based on density temperature (AR5_T_pDDrft, 196.2). Individually, each caused a 30–40 ppb CO decrease from the AR5 October mean, all of which were significant at the 95% level across ensemble members. The experiments with slightly higher entrainment coefficient (AR5_HighEntCoef) and less downdraft re-evaporation (AR5_LessDDrftRvp) were not significantly different from AR5. The experiment with all cumulus changes made simultaneously (AR5_CumulusChanges) was 76 ppbv lower than AR5 and constituted most of the difference between AR5 and AR5'.

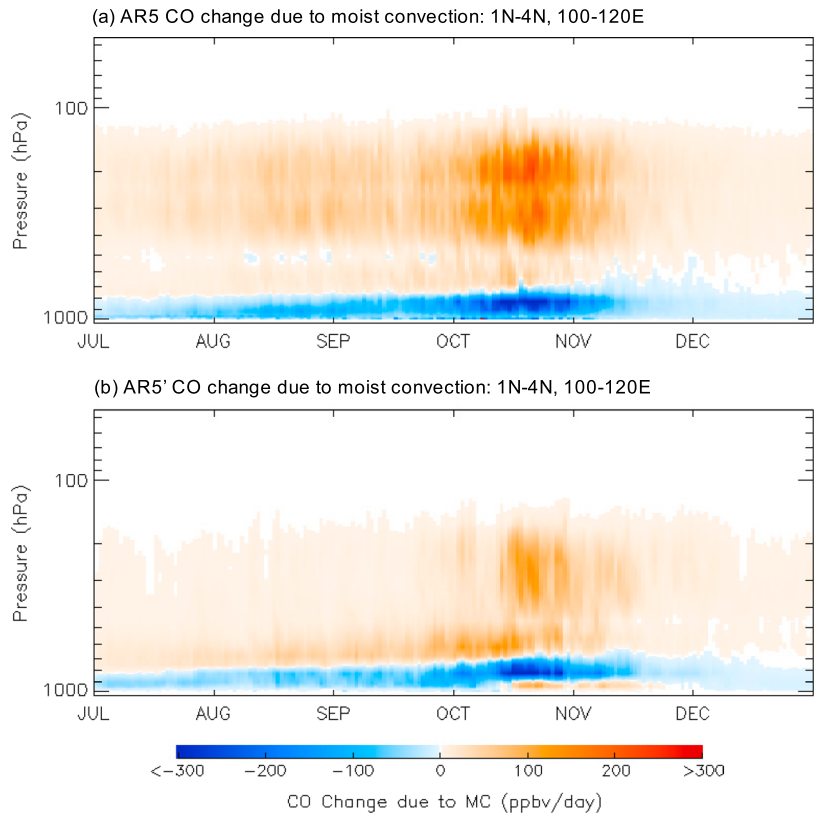


Figure 11. Same as Figure 10 but north of source region.

4. Discussion

There were large discrepancies between upper tropospheric Aura CO and the AR5 physics version of ModelE2, which should be viewed in the context of previous evaluations of ModelE. The AR4 version CO was 20 ppbv lower than MOPITT in the globally averaged midtroposphere over 2000–2004 [Shindell et al., 2006]. Over 2000–2006, the ModelE2 AR5 CO was 22 ppbv higher than MOPITT globally averaged midtroposphere [Naik et al., 2013]. This was consistent with the positive bias relative to TES identified by Voulgarakis et al. [2011], who attributed the change in bias direction from AR4 to AR5 to new anthropogenic emissions estimates and also to a possible low CO bias in TES.

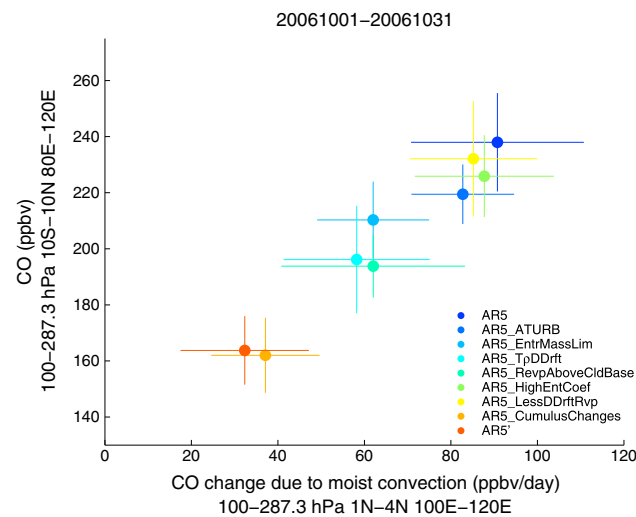


Figure 12. Regional CO vs. CO change due to convection north of source region across the nine ModelE2 experiments.

Over Indonesia in 2006, upper tropospheric CO in AR5 is unrealistically high (Figure 5) to a degree well beyond the known Aura biases. Based on this discrepancy, it would be justifiable to modify biomass burning emissions from Indonesia to bring the model and satellite estimates into better agreement. Bottom-up estimates of biomass burning emissions are uncertain, particularly in Indonesia due to a poor understanding of, and satellite detection issues related to, peat burning. Nassar et al. [2009] conducted GEOS-Chem simulations of the event using prescribed GFED v2 emissions, finding

Over Indonesia in 2006, upper tropospheric CO in AR5 is unrealistically high (Figure 5) to a degree well beyond the known Aura biases. Based on this discrepancy, it would be justifiable to modify biomass burning emissions from Indonesia to bring the model and satellite estimates into better agreement. Bottom-up estimates of biomass burning emissions are uncertain, particularly in Indonesia due to a poor understanding of, and satellite detection issues related to, peat burning. Nassar et al. [2009] conducted GEOS-Chem simulations of the event using prescribed GFED v2 emissions, finding

reasonable agreement with TES CO in the midtroposphere through October over western Indonesia. Into November, TES CO persisted at ~240 ppb, but GEOS-Chem decreased to ~160 ppb, effectively doubling GEOS-Chem's low CO bias relative to TES. They found better agreement by increasing GFED emissions over the source region by a factor of three in November 2006. Similarly, *Zhang et al.* [2011] found that at the event's peak, CO at 215 hPa was 40–50 ppb higher for GFED v3 than v2, due to the former's higher emissions.

What we have shown is that for this case, subgrid physics changes can change the vertical CO distribution to a degree comparable to large emissions changes made in other studies. In this case, ModelE2 CO with AR5' subgrid physics (Figure 8b) was brought into better agreement with Aura CO (Figure 6) through the depth of the troposphere. The AR5' CO is still higher than Aura CO during the peak of the event (Figure 5), but if we allow for a 25% Aura CO increase to ~150 ppb to account for its likely low bias, there is fairly close agreement between the model and satellite.

That convection played an important role in supplying CO from the surface to the upper troposphere is unsurprising. *Nassar et al.* [2009] found that significant CO is supplied convectively from the surface to the upper troposphere using experiments where tracer transport by deep convection was turned off. *Zhang et al.* [2011] also simulated the event using GEOS-Chem, comparing upper tropospheric CO concentrations for GEOS-4 and GEOS-5 prescribed meteorology. At 215 hPa, CO from the GEOS-4 simulation was 30–40 ppb greater than GEOS-5 during the peak of the event. *Liu et al.* [2013] found smaller differences in CO at 215 hPa over Indonesia in their comparison of GEOS-4 and GEOS-5 than *Zhang et al.* [2011], which could in part be due to differences in their western Indonesia analysis domains, but they did find significant differences elsewhere in the tropics.

Zhang et al. [2011] attributed the higher upper tropospheric CO for simulations with GEOS-4 to stronger deep convection inferred from simulated upper tropospheric ^{222}Rn in the zonal mean, and stronger convective precipitation and higher cloud top height over western Indonesia. Similarly, precipitation over the source region (Figure 2), as a general indicator of convective activity, was higher for AR5 compared to AR5', but the differences were small relative to much sharper gradients elsewhere in the region.

By looking in more detail at how the source strength, horizontal surface transport, and convective CO transport varied within a large domain over western Indonesia, we were able to understand how CO was supplied to the upper troposphere and how this differed between AR5 and AR5'. Either directly above the source region or after horizontal advection at the surface to the southern fringe of the model's ITCZ (Figure 9), parameterized convection plays a significant role in vertically redistributing CO in both simulations. Our interpretation of the differences in CO convective tendency between experiments is that during the period of interest, AR5' simulates convective towers that are weaker and shallower than those of AR5. The parameterization changes that are applied to AR5', especially those to the cumulus parameterization, generally affect the behavior of convection depending on the amount of environmental humidity. When the environment is dry, AR5' would produce weaker and shallower convective plumes than AR5 because its convective plumes entrain more subsaturated environmental air that would lead the plume to quickly lose its buoyancy. When the environment is humid enough (e.g., in a nearly saturated column), however, entraining more environmental air would not affect plume's buoyancy much but increase the convective mass flux, indicating stronger convection. During October, midtropospheric relative humidity in the source region and that north of the source region are lower for AR5' than AR5, but both remain mostly lower than 50% in both simulations (not shown). It is difficult to separate the subgrid and large-scale environmental influences on relative humidity, but for both cases, it is generally below 50%. This environmental condition—the effectively dry midtroposphere—might partially explain why convective plumes are shallower and weaker in AR5' than in AR5. Allowing more re-evaporation above cloud base also contributed to lower net upward CO transport (Figure 12), but at present a localized mechanism causing the change is not clear.

Ott et al. [2011] examined the sensitivity of modeled CO to perturbed subgrid physics for the GEOS5 with a free-running atmosphere forced only by observed sea-surface temperatures. For Indonesia, they examined SON 2002 during which emissions were much smaller than 2006 but still above average. GEOS-5 simulations with two representative convective configurations having minimum and maximum amounts of convective activity showed nearly identical amounts of CO up to 1 km over a region approximately the same as the source region defined in Figure 10. They found that when convection was reduced, large-scale vertical and horizontal mass flux compensated to remove CO from below 1 km. The eventual vertical fate was not examined for that case,

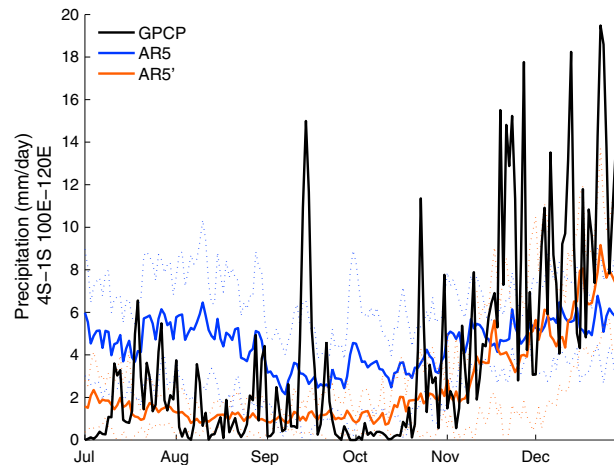


Figure 13. GPCP, AR5, and AR5' precipitation over source region.

and it is possible that there were different upper tropospheric CO levels for convection and slow, grid-scale ascent. But over a 4 year mean, seasonal zonal CO means were also fairly similar between the two end-members. The most likely reason for the greater vertical sensitivity to the physics changes in Table 1 for ModelE2 is our inclusion of more substantial structural changes compared to the single parameter adjustments that were examined exclusively by *Ott et al.* [2011] for GEOS-5. Another factor is our examination of the upper tropospheric CO response to a uniquely large emissions pulse. At a subseasonal timescale, differences in the effects of slow and fast vertical CO ascent would be more apparent.

Returning to a more conventional type of model evaluation, an obvious question is how the physics changes affected precipitation over the region, because a stronger than normal dry season was part of what caused the severe burning in the first place [*van der Werf et al.*, 2008; *Field and Shen*, 2008]. Over the source region in Figure 2b, mean AR5 precipitation from July to October was 4.1 mm/d compared to the 1.8 mm/d GPCP estimate (Figure 13). Mean July–October AR5' precipitation was 1.3 mm/d, slightly lower than GPCP but in better agreement. The difference between AR5 and AR5' mean precipitation for this period is significant at the 95% significance level across ensemble members, and the AR5' precipitation increase with the return of the monsoon also appears more realistic. Less AR5' precipitation during the July–November period is generally consistent with a May–November decrease in precipitation over the region in *Kim et al.* [2012] for the same cumulus changes over a 20 year mean. The lack of variance in the AR5 and AR5' compared to GPCP (Figure 13) is partly due to averaging across ensemble members. Less precipitation over the source region might suggest that less convection overall is contributing to a lower free-tropospheric CO for AR5 than AR5', in addition to a lower altitude of maximum convective CO tendency.

ModelE2 emissions are prescribed from GFED estimates in this study and will not respond to precipitation differences between the AR5 and AR5'. But as prognostic fire activity becomes more common in ModelE2 [*Pechony and Shindell*, 2009] and becomes more sophisticated for models in general [*Voulgarakis and Field*, 2015], it is useful to think about the dependence of prognostic fire estimates on uncertainty in other model components, with precipitation being among the most important. That the AR5' version of ModelE2 produces a realistic MJO is important given the possibility that its absence can influence fire activity in Indonesia [*Reid et al.*, 2012]. Identifying a different precipitation response to ENSO and Indian Ocean Dipole conditions between AR5 and AR5' would also be useful toward modeling strong interannual variability in biomass burning emissions.

5. Conclusions

For practical reasons, different parts of a composition-climate model are developed independently. The 70–80 ppbv difference in upper tropospheric CO over Indonesia in October 2006 between AR5 and AR5' versions of ModelE2 reinforces the need to consider all possible reasons for composition errors. *Naik et al.* [2013] found a strong positive bias in their multimodel mean CO in the midtroposphere over the tropics relative to MOPITT (see their Figure 2b). Discrepancies in biomass burning emissions were suggested as the reason, but their pattern of CO bias also corresponds roughly to tropical rainfall patterns, which suggests a convective influence. Any adjustments to emissions estimates, for example, could partially be compensating for other problems in the model. These effects have been shown for CTMs by comparing simulations using different reanalyses where a bulk set of physics changes have been implemented, or an entirely new cumulus scheme has been introduced. The intermediate CCM experiments between AR5 and AR5' conducted in this study show how a bulk set of physics changes can be examined individually to identify the most important

changes, which in the case of ModelE2's vertical CO distribution were a new entrainment mass limiter, more re-evaporation above cloud base, and a negative buoyancy threshold for downdraft initiation based on density temperature.

As in *Liu et al.* [2010], this work has implications for studies using inverse methods to estimate the uncertainty or biases in emissions. We showed that upper tropospheric CO could be reduced significantly by changing the vertical transport characteristics of the forward model. This does not preclude errors in estimated biomass burning emissions but reinforces the need to consider subgrid physics errors at the same time to account for different sources of uncertainty. In this case with the CCM, we are able to conduct individual experiments to identify the most important parameterization changes. In theory, one could estimate a distribution of different inversion estimates using an ensemble of similar experiments for a more comprehensive estimate of forward model transport error.

Conversely, this study hints at the potential for using trace gas measurements to evaluate model parameterizations alongside more conventional measurements, as has been suggested previously [*Folkens et al.*, 2006; *Livesey et al.*, 2013]. In that context, our comparison against Aura CO retrievals is an independent check on the physics changes proposed for different reasons, namely, the reasonable simulation of the MJO and slightly improved marine stratocumulus over the eastern oceans. In neither case were there dramatic improvements in mean precipitation state. But with the significant improvement in agreement with TES stable water isotope retrievals for a similar set of experiments [*Field et al.*, 2014], the improved vertical CO distribution for the case considered here does suggest that the underlying AR5' physics changes have fundamental advantages over those in AR5. As trace gas retrievals mature and their biases and errors become better characterized, they will become more useful as for model evaluation alongside more conventional measurements.

The underlying reasons for the differences between AR5 and AR5' CO warrant further attention. We diagnosed the net effects of parameterized convection, which in reality reflect the contributions of sometimes competing factors, such as the frequency of convection, updraft strength, detrainment height, and downward transport through downdrafts and compensating subsidence. A useful next step would be to diagnose and determine the relative importance of each in estimating a complete budget of CO variability. The effects of large-scale horizontal and vertical transport and chemical production and destruction should also be taken into account.

Future work should also broaden the experiments and diagnoses to include emissions and chemistry-related influences in a systematic way alongside the convective processes examined here. *Marlier et al.* [2014] illustrated the benefits of using GFED emissions estimates with daily temporal frequency for ModelE2, which could interact with the timing of the onset of deep convection to affect upper tropospheric CO in Figure 5, either positively or negatively. Three-hourly resolution biomass burning estimates are now available [*Mu et al.*, 2011], which could interact with the diurnal cycle of convection across different model versions. Because ModelE2 is a full complexity composition-climate model, we also cannot exclude the possibility that secondary chemical effects related to the convective changes are also playing a role on CO distribution, for example, convective influences on OH via effects on water vapor, ozone, and photolysis. Using chemical diagnostics that are more process oriented, such as the ozone-CO correlation, can also provide further insight into how differences in convection parameterizations may affect the chemical processing of emissions, given the possibly strong sensitivity of such a metric to the handling of vertical transport in models, as suggested by *Voulgarakis et al.* [2011].

We have also not examined the effects of the convective changes on aerosols or other important, measureable trace gases, and their agreement with observations, to determine if the AR5' improvements hold up for other quantities. Future work should include these comparisons. Conversely, although much uncertainty remains, emitted aerosols from fires in Indonesia (and in general) can affect regional radiation balance [*Podgorny et al.*, 2003; *Duncan et al.*, 2003], circulation [*Ott et al.*, 2010; *Tosca et al.*, 2010], and precipitation [*Langmann*, 2007; *Tosca et al.*, 2010] to different degrees depending on the relative amounts of organic and black carbon emitted. It would be useful to understand the magnitude of these effects for ModelE2, and their sensitivity to physics changes alongside uncertainty in the emissions and the model's cloud and aerosol microphysics. Lastly, extending the analysis to other years and across the tropics to include important low-latitude, pollutant source regions such as South Asia, tropical Africa, and the tropical Americas will be important to see if parameterization-dependent transport mechanisms are different outside of the Maritime Continent.

Acknowledgments

R.F. was supported by the NASA Atmospheric Chemistry Modeling and Analysis Program grant NNX13AD46G, D.K. by the NASA grant NNX13AM18G, and A.D.G. by the NASA Modeling and Analysis Program. AV thanks the European Commission's Marie Curie International Research Staff Exchange Scheme (IRSES) for funding under the project titled "Regional climate-air quality interactions (REQUA)". Research was partially supported by the Jet Propulsion Laboratory, California Institute of Technology under contract to the National Aeronautics and Space Administration (NASA). Resources supporting this work were provided by the NASA High-End Computing (HEC) Program through the NASA Center for Climate Simulation (NCCS) at Goddard Space Flight Center. All data in the study can be obtained by contacting the lead author.

References

- Abad, G. G., et al. (2011), Ethane, ethyne and carbon monoxide concentrations in the upper troposphere and lower stratosphere from ACE and GEOS-Chem: A comparison study, *Atmos. Chem. Phys.*, *11*(18), 9927–9941, doi:10.5194/acp-11-9927-2011.
- Andreae, M. O., et al. (2001), Transport of biomass burning smoke to the upper troposphere by deep convection in the equatorial region, *Geophys. Res. Lett.*, *28*(6), 951–954, doi:10.1029/2000GL012391.
- Arakawa, A. (2004), The cumulus parameterization problem: Past, present, and future, *J. Clim.*, *17*(13), 2493–2525, doi:10.1175/1520-0442(2004)017<2493:ratcpp>2.0.co;2.
- Chatfield, R. B., J. A. Vastano, L. Li, G. W. Sachse, and V. S. Connors (1998), The Great African plume from biomass burning: Generalizations from a three-dimensional study of TRACE A carbon monoxide, *J. Geophys. Res.*, *103*(D21), 28,059–28,077, doi:10.1029/97JD03363.
- Dickerson, R. R., et al. (1987), Thunderstorms—An important mechanism in the transport of air pollutants, *Science*, *235*(4787), 460–464, doi:10.1126/science.235.4787.460.
- Duncan, B. N., I. Bey, M. Chin, L. J. Mickley, T. D. Fairlie, R. V. Martin, and H. Matsueda (2003), Indonesian wildfires of 1997: Impact on tropospheric chemistry, *J. Geophys. Res.*, *108*(D15), 4458, doi:10.1029/2002JD003195.
- Edwards, D. P., et al. (2006), Satellite-observed pollution from Southern Hemisphere biomass burning, *J. Geophys. Res.*, *111*, D14312, doi:10.1029/2005JD006655.
- Field, R. D., and S. S. P. Shen (2008), Predictability of carbon emissions from biomass burning in Indonesia from 1997 to 2006, *J. Geophys. Res.*, *113*, G04024, doi:10.1029/2008JG000694.
- Field, R. D., G. R. van der Werf, and S. S. P. Shen (2009), Human amplification of drought-induced biomass burning in Indonesia since 1960, *Nat. Geosci.*, *2*(3), 185–188, doi:10.1038/ngeo443.
- Field, R. D., D. Kim, A. L. LeGrande, J. Worden, M. Kelley, and G. A. Schmidt (2014), Evaluating climate model performance in the tropics with retrievals of water isotopic composition from Aura TES, *Geophys. Res. Lett.*, *41*, 6030–6036, doi:10.1002/2014GL060572.
- Folkens, I., P. Bernath, C. Boone, L. J. Donner, A. Eldering, G. Lesins, R. V. Martin, B. M. Sinnhuber, and K. Walker (2006), Testing convective parameterizations with tropical measurements of HNO₃, CO, H₂O, and O-3: Implications for the water vapor budget, *J. Geophys. Res.*, *111*, D23304, doi:10.1029/2006JD007325.
- Holtstlag, A. A. M., and B. A. Boville (1993), Local versus nonlocal boundary-layer diffusion in a global climate model, *J. Clim.*, *6*(10), 1825–1842, doi:10.1175/1520-0442(1993)006<1825:lvnblnd>2.0.co;2.
- Holtstlag, A. A. M., and C. H. Moeng (1991), Eddy diffusivity and countergradient transport in the convective atmospheric boundary layer, *J. Atmos. Sci.*, *48*(14), 1690–1698, doi:10.1175/1520-0469(1991)048<1690:edacti>2.0.co;2.
- Huang, L., R. Fu, J. H. Jiang, J. S. Wright, and M. Luo (2012), Geographic and seasonal distributions of CO transport pathways and their roles in determining CO centers in the upper troposphere, *Atmos. Chem. Phys.*, *12*(10), 4683–4698, doi:10.5194/acp-12-4683-2012.
- Jiang, J. H., N. J. Livesey, H. Su, L. Neary, J. C. McConnell, and N. A. D. Richards (2007), Connecting surface emissions, convective uplifting, and long-range transport of carbon monoxide in the upper troposphere: New observations from the Aura Microwave Limb Sounder, *Geophys. Res. Lett.*, *34*, L18812, doi:10.1029/2007GL030638.
- Kim, D., A. H. Sobel, A. D. Del Genio, Y. H. Chen, S. J. Camargo, M. S. Yao, M. Kelley, and L. Nazarenko (2012), The tropical subseasonal variability simulated in the NASA GISS general circulation model, *J. Clim.*, *25*(13), 4641–4659, doi:10.1175/jcli-d-11-00447.1.
- Koch, D., G. A. Schmidt, and C. V. Field (2006), Sulfur, sea salt, and radionuclide aerosols in GISS ModelE, *J. Geophys. Res.*, *111*, D06206, doi:10.1029/2004JD005550.
- Koch, D., T. C. Bond, D. Streets, and N. Unger (2007), Linking future aerosol radiative forcing to shifts in source activities, *Geophys. Res. Lett.*, *34*, L05821, doi:10.1029/2006GL028360.
- Lai, S. C., A. K. Baker, T. J. Schuck, F. Slemr, C. A. M. Brenninkmeijer, P. van Velthoven, D. E. Oram, A. Zahn, and H. Ziereis (2011), Characterization and source regions of 51 high-CO events observed during Civil Aircraft for the Regular Investigation of the Atmosphere Based on an Instrument Container (CARIBIC) flights between south China and the Philippines, 2005–2008, *J. Geophys. Res.*, *116*, D20308, doi:10.1029/2011JD016375.
- Lamarque, J. F., et al. (2010), Historical (1850–2000) gridded anthropogenic and biomass burning emissions of reactive gases and aerosols: Methodology and application, *Atmos. Chem. Phys.*, *10*(15), 7017–7039, doi:10.5194/acp-10-7017-2010.
- Langmann, B. (2007), A model study of smoke-haze influence on clouds and warm precipitation formation in Indonesia 1997/1998, *Atmos. Environ.*, *41*(32), 6838–6852, doi:10.1016/j.atmosenv.2007.04.050.
- Liu, J., J. A. Logan, L. T. Murray, H. C. Pumphrey, M. J. Schwartz, and I. A. Megretskaja (2013), Transport analysis and source attribution of seasonal and interannual variability of CO in the tropical upper troposphere and lower stratosphere, *Atmos. Chem. Phys.*, *13*(1), 129–146, doi:10.5194/acp-13-129-2013.
- Liu, J. H., J. A. Logan, D. B. A. Jones, N. J. Livesey, I. Megretskaja, C. Carouge, and P. Nedelec (2010), Analysis of CO in the tropical troposphere using Aura satellite data and the GEOS-Chem model: Insights into transport characteristics of the GEOS meteorological products, *Atmos. Chem. Phys.*, *10*(24), 12,207–12,232, doi:10.5194/acp-10-12207-2010.
- Livesey, N. J., J. A. Logan, M. L. Santee, J. W. Waters, R. M. Doherty, W. G. Read, L. Froidevaux, and J. H. Jiang (2013), Interrelated variations of O-3, CO and deep convection in the tropical/subtropical upper troposphere observed by the Aura Microwave Limb Sounder (MLS) during 2004–2011, *Atmos. Chem. Phys.*, *13*(2), 579–598, doi:10.5194/acp-13-579-2013.
- Logan, J. A., I. Megretskaja, R. Nassar, L. T. Murray, L. Zhang, K. W. Bowman, H. M. Worden, and M. Luo (2008), Effects of the 2006 El Niño on tropospheric composition as revealed by data from the Tropospheric Emission Spectrometer (TES), *Geophys. Res. Lett.*, *35*, L03816, doi:10.1029/2007GL031698.
- Luo, M., W. Read, S. Kulawik, J. Worden, N. Livesey, K. Bowman, and R. Herman (2013), Carbon monoxide (CO) vertical profiles derived from joined TES and MLS measurements, *J. Geophys. Res. Atmos.*, *118*, 10,601–10,613, doi:10.1002/jgrd.50800.
- Luo, M., M. Schwartz, W. Read, R. Herman, S. Kulawik, J. Worden, N. Livesey, K. Bowman, and C. Sweeney (2014), Introducing and validating the new Aura CO product derived from joined TES and MLS measurements, in *AGU Fall Meeting*, edited, San Francisco, Calif.
- Marlier, M. E., A. Voulgarakis, D. T. Shindell, G. Faluvegi, C. L. Henry, and J. T. Randerson (2014), The role of temporal evolution in modeling atmospheric emissions from tropical fires, *Atmos. Environ.*, *89*, 158–168, doi:10.1016/j.atmosenv.2014.02.039.
- Mu, M., et al. (2011), Daily and 3-hourly variability in global fire emissions and consequences for atmospheric model predictions of carbon monoxide, *J. Geophys. Res.*, *116*, D24303, doi:10.1029/2011JD016245.
- Naik, V., et al. (2013), Preindustrial to present-day changes in tropospheric hydroxyl radical and methane lifetime from the Atmospheric Chemistry and Climate Model Intercomparison Project (ACCMIP), *Atmos. Chem. Phys.*, *13*(10), 5277–5298, doi:10.5194/acp-13-5277-2013.
- Nakanishi, M. (2001), Improvement of the Mellor-Yamada turbulence closure model based on large-eddy simulation data, *Boundary Layer Meteorol.*, *99*(3), 349–378, doi:10.1023/a:1018915827400.

- Nassar, R., J. A. Logan, I. A. Megretskaya, L. T. Murray, L. Zhang, and D. B. A. Jones (2009), Analysis of tropical tropospheric ozone, carbon monoxide, and water vapor during the 2006 El Niño using TES observations and the GEOS-Chem model, *J. Geophys. Res.*, *114*, D17304, doi:10.1029/2009JD011760.
- Ott, L., B. Duncan, S. Pawson, P. Colarco, M. Chin, C. Randles, T. Diehl, and E. Nielsen (2010), Influence of the 2006 Indonesian biomass burning aerosols on tropical dynamics studied with the GEOS-5 AGCM, *J. Geophys. Res.*, *115*, D14121, doi:10.1029/2009JD013181.
- Ott, L., S. Pawson, and J. Bacmeister (2011), An analysis of the impact of convective parameter sensitivity on simulated global atmospheric CO distributions, *J. Geophys. Res.*, *116*, D21310, doi:10.1029/2011JD016077.
- Park, M., W. J. Randel, D. E. Kinnison, L. K. Emmons, P. F. Bernath, K. A. Walker, C. D. Boone, and N. J. Livesey (2013), Hydrocarbons in the upper troposphere and lower stratosphere observed from ACE-FTS and comparisons with WACCM, *J. Geophys. Res. Atmos.*, *118*, 1964–1980, doi:10.1029/2012JD018327.
- Pechony, O., and D. T. Shindell (2009), Fire parameterization on a global scale, *J. Geophys. Res.*, *114*, D16115, doi:10.1029/2009JD011927.
- Pickering, K. E., et al. (1996), Convective transport of biomass burning emissions over Brazil during TRACE A, *J. Geophys. Res.*, *101*(D19), 23,993–24,012, doi:10.1029/96JD00346.
- Podgorny, I. A., F. Li, and V. Ramanathan (2003), Large aerosol radiative forcing due to the 1997 Indonesian forest fire, *Geophys. Res. Lett.*, *30*(1), 1028, doi:10.1029/2002GL015979.
- Reichle, H. G., V. S. Connors, J. A. Holland, W. D. Hypes, H. A. Wallio, J. C. Casas, B. B. Gormsen, and M. S. Saylor (1986), Middle and upper tropospheric carbon-monoxide mixing ratios as measured by a satellite-borne remote sensor during November 1981, *J. Geophys. Res.*, *91*(D10), 865–887, doi:10.1029/JD091iD10p10865.
- Reid, J. S., P. Xian, E. J. Hyer, M. K. Flatau, E. M. Ramirez, F. J. Turk, C. R. Sampson, C. Zhang, E. M. Fukada, and E. D. Maloney (2012), Multi-scale meteorological conceptual analysis of observed active fire hotspot activity and smoke optical depth in the Maritime Continent, *Atmos. Chem. Phys.*, *12*(4), 2117–2147, doi:10.5194/acp-12-2117-2012.
- Roths, J., and G. W. Harris (1996), The tropospheric distribution of carbon monoxide as observed during the TROPOZ II experiment, *J. Atmos. Chem.*, *24*(2), 157–188, doi:10.1007/bf00162409.
- Schmidt, G. A., et al. (2014), Configuration and assessment of the GISS ModelE2 contributions to the CMIP5 archive, *J. Adv. Model. Earth Syst.*, *6*, 141–184, doi:10.1002/2013ms000265.
- Seiler, W., and J. Fishman (1981), The distribution of carbon-monoxide and ozone in the free troposphere, *J. Geophys. Res.*, *86*(NC8), 7255–7265, doi:10.1029/JC086iC08p07255.
- Sherwood, S. C., S. Bony, and J. L. Dufresne (2014), Spread in model climate sensitivity traced to atmospheric convective mixing, *Nature*, *505*(7481), 37–42, doi:10.1038/nature12829.
- Shindell, D. T., et al. (2006), Multimodel simulations of carbon monoxide: Comparison with observations and projected near-future changes, *J. Geophys. Res.*, *111*, D19306, doi:10.1029/2006JD007100.
- Shindell, D. T., et al. (2013), Interactive ozone and methane chemistry in GISS-E2 historical and future climate simulations, *Atmos. Chem. Phys.*, *13*(5), 2653–2689, doi:10.5194/acp-13-2653-2013.
- Tosca, M. G., J. T. Randerson, C. S. Zender, M. G. Flanner, and P. J. Rasch (2010), Do biomass burning aerosols intensify drought in equatorial Asia during El Niño?, *Atmos. Chem. Phys.*, *10*(8), 3515–3528.
- van der Werf, G. R., et al. (2008), Climate regulation of fire emissions and deforestation in equatorial Asia, *Proc. Natl. Acad. Sci. U.S.A.*, *105*(51), 20,350–20,355, doi:10.1073/pnas.0803375105.
- van der Werf, G. R., J. T. Randerson, L. Giglio, G. J. Collatz, M. Mu, P. S. Kasibhatla, D. C. Morton, R. S. DeFries, Y. Jin, and T. T. van Leeuwen (2010), Global fire emissions and the contribution of deforestation, savanna, forest, agricultural, and peat fires (1997–2009), *Atmos. Chem. Phys.*, *10*(23), 11,707–11,735, doi:10.5194/acp-10-11707-2010.
- Voulgarakis, A., and R. D. Field (2015), Fire influences on atmospheric composition, air quality, and climate, *Curr. Pollut. Rep.*, doi:10.1007/s40726-015-0007-z.
- Voulgarakis, A., P. J. Telford, A. M. Aghedo, P. Braesicke, G. Faluvegi, N. L. Abraham, K. W. Bowman, J. A. Pyle, and D. T. Shindell (2011), Global multi-year O₃-CO correlation patterns from models and TES satellite observations, *Atmos. Chem. Phys.*, *11*(12), 5819–5838, doi:10.5194/acp-11-5819-2011.
- Voulgarakis, A., et al. (2013), Analysis of present day and future OH and methane lifetime in the ACCMIP simulations, *Atmos. Chem. Phys.*, *13*(5), 2563–2587, doi:10.5194/acp-13-2563-2013.
- Wild, O., X. Zhu, and M. J. Prather (2000), Fast-j: Accurate simulation of in- and below-cloud photolysis in tropospheric chemical models, *J. Atmos. Chem.*, *37*(3), 245–282, doi:10.1023/a:1006415919030.
- Worden, J., et al. (2013), El Niño, the 2006 Indonesian peat fires, and the distribution of atmospheric methane, *Geophys. Res. Lett.*, *40*, 4938–4943, doi:10.1002/grl.50937.
- Yao, M. S., and Y. Cheng (2012), Cloud simulations in response to turbulence parameterizations in the GISS Model E GCM, *J. Clim.*, *25*(14), 4963–4974, doi:10.1175/jcli-d-11-00399.1.
- Zhang, L., Q. B. Li, J. Jin, H. Liu, N. Livesey, J. H. Jiang, Y. Mao, D. Chen, M. Luo, and Y. Chen (2011), Impacts of 2006 Indonesian fires and dynamics on tropical upper tropospheric carbon monoxide and ozone, *Atmos. Chem. Phys.*, *11*(21), 10,929–10,946, doi:10.5194/acp-11-10929-2011.